Pergamon

Neuroscience Vol. 92, No. 2, pp. 445–457, 1999

PII: S0306-4522(98)00759-3
0306-4522/99 $20.00+0.00

PROPERTIES OF A HYPERPOLARIZATION-ACTIVATED CATION CURRENT IN INTERNEURONS IN THE RAT LATERAL GENICULATE NUCLEUS

J. J. ZHU,*†‡ D. J. UHLRICH* and W. W. LYTTON*

*Departments of Anatomy, Neurology and Neuroscience Training program, University of Wisconsin Medical School and Wm. S. Middleton VA Hospital, 1300 University Avenue, Madison, WI 53706, U.S.A.

†Marine Biological Laboratory, Woods Hole, MA 02543, U.S.A.

Abstract—A hyperpolarization-activated cation conductance contributes to the membrane properties of a variety of cell types. In the thalamus, a prominent hyperpolarization-activated cation conductance exists in thalamocortical cells, and this current is implicated in the neuromodulation of complex firing behaviors. In contrast, the GABAergic cells in the reticular nucleus in the thalamus appear to lack this conductance. The presence and role of this cation conductance in the other type of thalamic GABAergic cells, local interneurons, is still unclear. To resolve this issue, we studied 54 physiologically and morphologically identified local interneurons in the rat dorsal lateral geniculate nucleus using an *in vitro* whole-cell patch recording technique. We found that hyperpolarizing current injections induced depolarizing voltage sags in these geniculate interneurons. The *I–V* relationship revealed an inward rectification. Voltage-clamp study indicated that a slow, hyperpolarization-activated cation conductance was responsible for the inward rectification. We then confirmed that this slow conductance had properties of the hyperpolarization-activated cation conductance described in other cell types. The slow conductance was insensitive to 10 mM tetraethylammonium and 0.5 mM 4-aminopyridine, but was largely blocked by 1–1.5 mM Cs^+. It was permeable to both K^+ and Na^+ ions and had a reversal potential of −44 mV. The voltage dependence of the hyperpolarization-activated cation conductance in interneurons was also studied: the activation threshold was about −55 mV, half-activation potential was about −80 mV and maximal conductance was about 1 nS. The activation and deactivation time constants of the conductance ranged from 100 to 1000 ms, depending on membrane potential. The depolarizing voltage sags and *I–V* relationship were further simulated in a model interneuron, using the parameters of the hyperpolarization-activated cation conductance obtained from the voltage-clamp study. The time-course and voltage dependence of the depolarizing voltage sags and *I–V* relationship in the model cell were very similar to those found in geniculate interneurons in current clamp.

Taken together, the results of the present study suggest that thalamic local interneurons possess a prominent hyperpolarization-activated cation conductance, which may play important roles in determining basic membrane properties and in modulating firing patterns. © 1999 IBRO. Published by Elsevier Science Ltd.

Key words: thalamus, thalamic reticular nucleus, intrinsic properties, inhibition, simulation, anomalous rectifier.

In mammals, the thalamus plays an important role in the transmission of sensory signals to cortex.[46,47] It is clear that inhibitory mechanisms contribute significantly toward determining the character of the ascending sensory signal, altering the time-course of sensory responses as well as the tuning of sensory receptive field properties.[2,3,36,54,61,62] Inhibitory mechanisms also play a role in a second major thalamic function; they contribute to the genesis and synchronization of oscillatory activity,[52] and inhibitory mechanisms have been implicated in the manifestation of aberrant oscillations of epilepsy.[25,49,52,55,56]

Thalamic functions are mediated largely by three basic cell types.[27] Thalamocortical cells are excitatory neurons, and they alone project to the cortex. Inhibition in the thalamus arises primarily from two GABAergic neurons:[27] interneurons and cells in the thalamic reticular nucleus (TRN), which reside respectively within and adjacent to the thalamic nuclei. Both interneurons and TRN cells innervate thalamocortical cells and shape the signal that is sent to the cortex. The nature of this inhibitory shaping depends in part on the response properties of the interneurons and TRN cells. Numerous studies of the electrophysiological properties of TRN cells have shown that they are endowed with active

‡To whom correspondence should be addressed at: Department of Cell Physiology, Max-Planck Institute for Medical Research, Jahnstr. 29, Heidelberg D-69120, Germany.

Abbreviations: EGTA, ethyleneglycolbis(aminoethyl ether) tetra-acetate; HEPES, *N*-2-hydroxyethylpiperazine-*N*∼-2-ethanesulfonic acid; I_h, hyperpolarization-activated cation conductance; I_{leak}, leak conductance; I_T, low-threshold calcium conductance; LGN, lateral geniculate nucleus; TRN, thalamic reticular nucleus.

membrane conductances that alter their firing behavior.[4,5,10,24] In contrast, interneurons have been little studied, and until recently, the membrane properties of interneurons were thought to be largely linear,[48] suggesting a relatively simple contribution to thalamic function. It is now clear that the inhibitory role of interneurons can be more complex. For example, like thalamocortical and TRN cells, interneurons are endowed with the voltage-dependent low-threshold calcium conductance, I_T.[43,65] This conductance can produce highly non-linear burst responses.[26,65]

Another voltage-dependent conductance, a hyperpolarization-activated cation conductance (I_h), is also heavily involved in regulating the neuronal firing properties. I_h has been implicated in altering the level of many fundamental membrane properties of neurons, such as resting membrane potential and input resistance, and it is also involved in more complex patterns of activity, including modulating the amplitude and time-course of postsynaptic responses, altering integrative ability, and pacing the frequency of oscillations.[18,29,33,50] In addition, I_h kinetics are regulated by many neurotransmitters.[40] This makes the role of I_h in thalamic cells particularly important, since thalamic firing patterns can be dramatically altered by neurotransmitters.[31]

While previous studies have shown that thalamocortical cells are richly endowed with I_h channels, and TRN cells lack them,[5,10,33] the prevalence of I_h in interneurons is unclear. Earlier work concluded that interneurons lacked I_h,[28] but recent studies have demonstrated a depolarizing "sag" of membrane potential in some interneurons, as well as an inwardly rectifying I–V relationship.[32,42,58] Though suggestive of I_h, these studies did not further characterize the conductance underlying the observed responses. Further, the depolarizing sag and inward rectification reported in the interneurons was small and inconsistent, which may reflect the effects of sharp electrode impalement.[51] This issue warrants further study, given the importance of inhibition to thalamic function and the limited information about the basic membrane and firing properties of thalamic interneurons. Thus, in the present study, we used the whole-cell recording technique to study the hyperpolarization-evoked responses in physiologically and morphologically identified local interneurons in the rat dorsal lateral geniculate nucleus (LGN).

EXPERIMENTAL PROCEDURES

Physiology

Experiments were performed in thalamic slices from four- to 10-week-old Sprague–Dawley rats (100–300 g; Harlan Sprague Dawley). All efforts were made to minimize suffering and the number of animals used. The rats were deeply anesthetized by halothane and decapitated. The brain was quickly removed into cold (6–8°C) physiological solution containing (in mM): NaCl 126, KCl 2.5, NaH_2PO_4 1.25, $NaHCO_3$ 26, $MgSO_4$ 1, dextrose 20, $CaCl_2$ 2, at pH 7.35. The solution was continuously bubbled with 95% O_2/5% CO_2. Slices containing the LGN, each 500 μm thick, were cut from the tissue blocks with a DTK-1000 microslicer (Dosaka Em Co.). These slices were kept in oxygenated physiological solution for at least 2 h before recording. During the recording, slices were submerged in a Plexiglas chamber and stabilized using a fine nylon net attached to a platinum ring. The chamber was perfused with warmed and oxygenated physiological solution, and the half-time for the bath solution exchange was about 7 s. The temperature of the bath solution in the chamber was kept at 34.0 ± 0.5°C. All antagonists were bath-applied.

The whole-cell recording technique[7,13,19] was used in this study. Patch electrodes were made from borosilicate tubing and their resistances were 7–9 MΩ with the intracellular solution. The standard intracellular solution (in mM) was: potassium gluconate 120, HEPES 10, EGTA 5, $MgCl_2$ 2, ATP 4, GTP 0.1, $CaCl_2$ 0.5, KCl 10 and 0.25% biocytin, at pH 7.25. A 10-mV liquid junction potential was subtracted from all membrane potentials. An Axoclamp-2A amplifier (Axon Instruments) was used to perform both current-clamp and voltage-clamp recordings. The electrode capacitance and series resistance compensation was made in discontinuous current-clamp mode, with the head stage output monitored continuously on a second oscilloscope. The series resistance was then read directly from the amplifier, while the input resistance was estimated by measuring the voltage change in response to a small hyperpolarizing current. Single-electrode continuous voltage-clamp study was performed only on the cells with low access resistance, ranging from 15 to 30 MΩ (20.4 ± 3.7 MΩ; mean ± S.D.). During the voltage-clamp study, access resistance was compensated with sourcing or sinking excess current, which effectively pushes the voltage beyond that measured through the electrode by manually programming or by using the internal compensation circuit of the Axoclamp 2A amplifier. Access resistance compensation of 70–85% was routinely achieved (cf. Ref. 24). Unless stated otherwise, 4 μM tetrodotoxin, 500 μM 4-aminopyridine, 10 mM tetraethylammonium and 400 μM Ni^{2+} were included in the bath solution during the voltage-clamp recordings. Currents were often averaged three times to increase the signal-to-noise ratio. After recordings, slices were fixed by immersion in 4% paraformaldehyde in 0.1 M phosphate buffer, resectioned, histologically reacted for biocytin[21] and subsequently drawn with the aid of a camera lucida system. All chemicals were purchased from Sigma.

Computer modeling

Computer modeling was performed on a Sun workstation using NEURON.[20] The model interneuron had 15 cylindrical compartments, representing a soma, two equivalent proximal dendrites and 12 equivalent distal dendrites. Diameters (D) and lengths (L) of these cylinders, estimated from stained geniculate interneurons and adjusted to fit the membrane time constant $\tau = 95$ ms, are listed below:

$D_{soma} = 10$ μm and $L_{soma} = 16$ μm;
$D_{proximal\ dendrite} = 3.25$ μm and $L_{proximal\ dendrite} = 240$ μm;
$D_{distal\ dendrite} = 1.75$ μm and $L_{distal\ dendrite} = 180$ μm.

As with previous modeling studies,[12,30,53] the specific membrane capacitance (C_m) and cytoplasmic resistance (R_i) for the model cell were set to be 1 μF/cm^2 and 100 Ω cm, respectively.

The model cell was equipped with a Hodgkin–Huxley style conductance (I_h) and a leak conductance (I_{leak}). Thus, the model can be described by the following equation:

$$C_m dV/dt = -I_{leak} - I_h + I_{inj}, \quad (1)$$

where C_m is the specific membrane capacitance and I_{inj} the injected current from the soma.

The leak current, I_{leak}, is described as

$$I_{leak} = g_{leak}(V - E_{leak}), \quad (2)$$

where $g_{leak} = 0.008$ mS/cm^2 is the conductance and $E_{leak} = -72.5$ mV the reversal potential.

The hyperpolarization-activated cation current, I_h, is described as

$$I_h = g_h h_\infty (V - E_h) \quad (3)$$

$$dh/dt = [h_\infty(V) - h]/\tau_h(V), \quad (4)$$

where $g_h = 0.03$–0.37 mS/cm^2 is the maximal conductance, $E_h = -44$ mV is the reversal potential,

$$h_\infty(V) = 1/\{1 + \exp[(V + 79)/7.4]\}$$

and

$$\tau_h(V) = \exp[(V + 293.3)/29.7]/\{1 + \exp[(V + 76.7)/7.8]\}.$$

These values were determined based on the voltage-clamp data (see Results section).

I_{leak} was inserted uniformly in the soma and dendrites. Since the distribution of I_h in the subcellular compartments in geniculate interneurons is unclear, I_h was only inserted in the soma to simplify the simulation. The maximal conductances of these two currents and reversal potential of I_{leak} were adjusted so that the model cell had a resting membrane potential of -69 mV and input resistance of 600 MΩ. The ratio of these two conductance-mediated inward currents, evoked by a voltage step from -60 to -100 mV, was kept at 2:1.

The time step for the simulations was typically set at 0.025 ms. Sometimes, a shorter time step (e.g., 0.01 or 0.005 ms) was also used to repeat the simulations. The results were nearly identical.

RESULTS

Neuronal identification

A hyperpolarization-activated cation conductance was studied in 54 interneurons in the rat LGN. The recordings usually lasted 1–4 h and cells typically showed no consistent sustained change in resting membrane potential or input resistance throughout the experiment. Our previous study has demonstrated that geniculate interneurons, when recorded with patch pipettes, exhibit a dramatically higher input resistance and a longer membrane time constant than relay cells.[63] These two properties are sufficient to unambiguously distinguish interneurons from relay cells. In this study, the same criteria (i.e. input resistance larger than 300 MΩ and/or time constant longer than 50 ms) were used to identify interneurons prior to subsequent morphological confirmation (Fig. 1B). For these interneurons the input resistance was 605 ± 209 MΩ, the time constant was 93.1 ± 24.2 ms and the resting membrane potential was -68.6 ± 4.8 mV.

The morphology of all 54 interneurons was recovered, which confirmed that the recordings were obtained from interneurons.[15–17,37,38,57,58] A representative morphological example is illustrated in Fig. 1A. It has a bipolar appearance, with two dendrites arising from a small soma. The dendrites, which are beaded and have intricate branching patterns, encompass a relatively large area within the LGN (Fig. 1C). In most interneurons, an axon originated from the soma or proximal dendrite and ramified locally in the LGN. The axonal and dendritic arbors tended to be spatially offset from each other, with the axon arbor occupying a relatively smaller area near the soma.

Presence of I_h in interneurons

We determined the I–V relationship by examining their responses to depolarizing and hyperpolarizing current steps (Fig. 2). The large hyperpolarization caused sags of membrane potential back toward the resting membrane potential during the later portion of the current step ($n = 33$; Fig. 2A). The I–V relationship at this late point of the hyperpolarization revealed a prominent inward rectification (Fig. 2B), which was observed consistently in all 33 cells. The derivation of the I–V curve from the linear relationship typically started at about -60 mV and increasingly deviated with greater hyperpolarizations, suggesting an underlying voltage-dependent conductance activated at about -60 mV.

Voltage-clamp study was then performed to determine the cellular mechanism underlying the inward rectification in 28 interneurons. In voltage-clamp mode, these cells responded to hyperpolarizing voltage steps with slowly activated inward currents (Fig. 3A). The result suggests that a slow hyperpolarization-activated conductance was responsible for the non-linear I–V relationship.

The slow kinetics of the inward currents suggest that the underlying conductance might be I_h.[40] This idea was tested with pharmacological approaches (Fig. 3). Bath application of 500 μM 4-aminopyridine and 10 mM tetraethylammonium had little effect on the inward current (not illustrated). However, when cesium (Cs^+; 1–1.5 mM), a potent I_h blocker,[40] was applied to the bath solution, it blocked the slow inward currents ($n = 3$; Fig. 3B). The Cs^+ application also revealed that I_{leak} in interneurons was voltage independent, since the instantaneous current increased linearly with the increase in hyperpolarization. After washing out Cs^+, the slow inward currents recovered (Fig. 3C). The results thus suggest that the slow inward currents are mediated by I_h.

To confirm the idea that the slow inward currents were mediated by I_h, a cation conductance,[59] the ion selectivity of the conductance was investigated by changing the extracellular concentration of K^+ and Na^+ (Fig. 4). After the control currents were obtained by hyperpolarizing voltage steps in the normal bath solution (Fig. 4A), the extracellular K^+ was increased from 2.5 to 7.5 mM. This manipulation increased the amplitudes of inward currents ($n = 4$; Fig. 4B). The control currents recovered after washing in the normal bath solution (Fig. 4C). In the

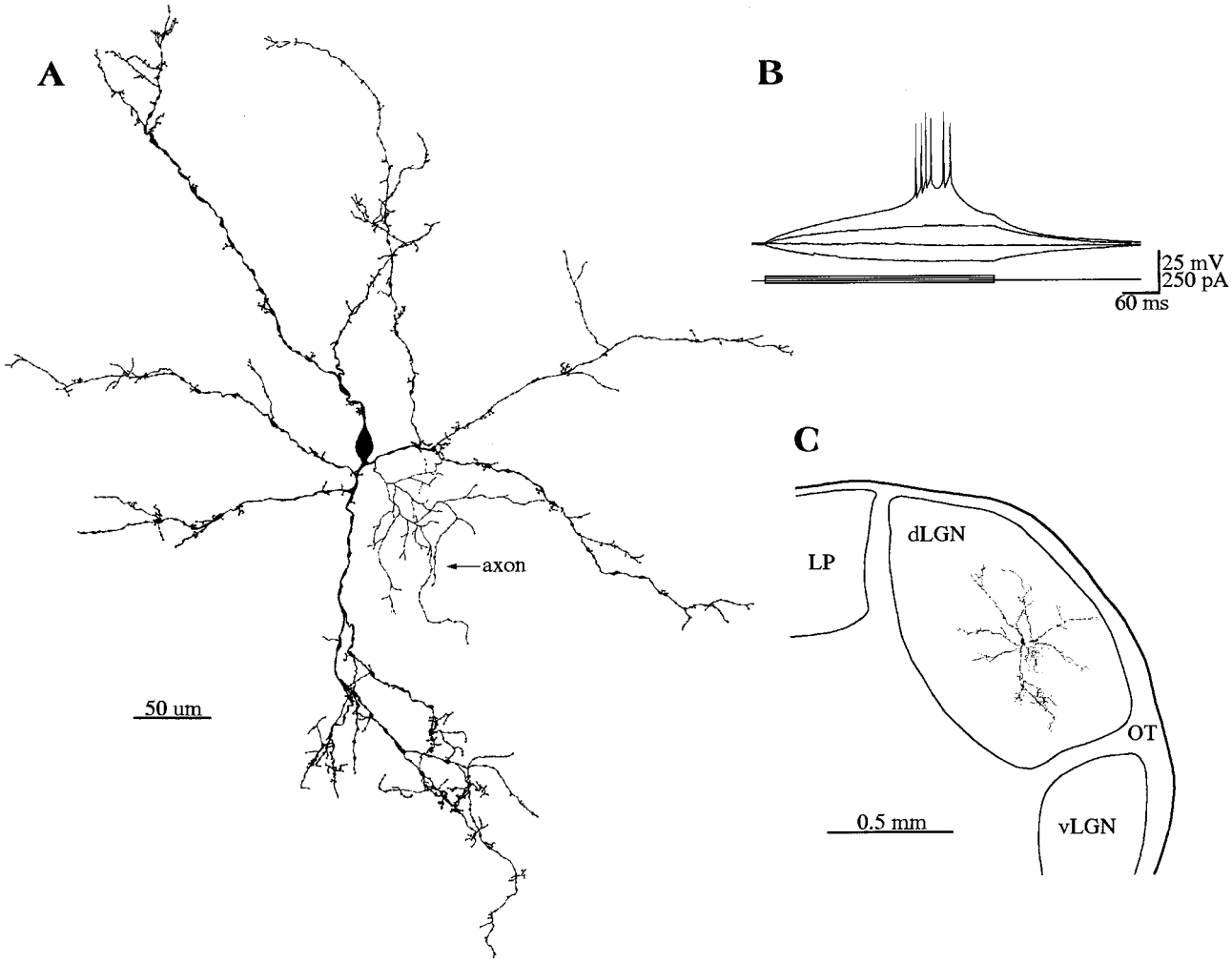

Fig. 1. Characterization of a geniculate interneuron. (A) Morphology of a geniculate interneuron, reconstructed by camera lucida. (B) Responses of the same interneuron to depolarizing and hyperpolarizing current pulses. The resting potential of this cell was − 73 mV and the access resistance of the recording was 18 MΩ. (C) Location of the cell in the LGN.

same experiment, extracellular Na^+ concentration was then decreased from 153 to 39 mM by substituting extracellular Na^+ ions with $NMDG^+$ ions. The manipulation decreased the amplitudes of inward currents ($n=4$; Fig. 4D). The control currents again recovered after washing in the normal bath solution (Fig. 4E). Together, the results indicate that the slow inward currents carry both K^+ and Na^+ ions, supporting the idea that I_h is responsible for the non-linear *I–V* relationship found in interneurons. This experiment also suggested that I_{leak} carried both K^+ and Na^+ ions in interneurons, since the instantaneous currents were sensitive to the changes in extracellular K^+ and Na^+ concentrations (Fig. 4F).

Reversal potential of I_h in interneurons

We also measured the reversal potential of I_h, using two different methods (Fig. 5). One way to estimate the reversal potential is by measuring the instantaneous *I–V* relationships at different holding potentials (cf. Ref. 6). Since the instantaneous current consists only of I_h and a linear leakage current (see Fig. 3), the instantaneous *I–V* relationships obtained at different holding potentials will intersect at the point where the driving force for I_h is zero (i.e. $V_m = E_h$). Figure 5A–D shows an example of how this method gave an estimated reversal potential of I_h in an interneuron. The cell was initially held at −60, −65 or −70 mV before being stepped to a series of potentials from −55 to −105 mV. The instantaneous currents in response to the voltage steps were then measured to obtain the *I–V* relationships. The *I–V* relationships were linear, consistent with the fact that I_{leak} in interneurons was a linear conductance, and intersected at about −47 mV, which was the reversal potential of I_h for this cell. The mean reversal potential of the I_h estimated by this measure in four interneurons was -44.7 ± 2.9 mV.

The reversal potential of I_h was also obtained by

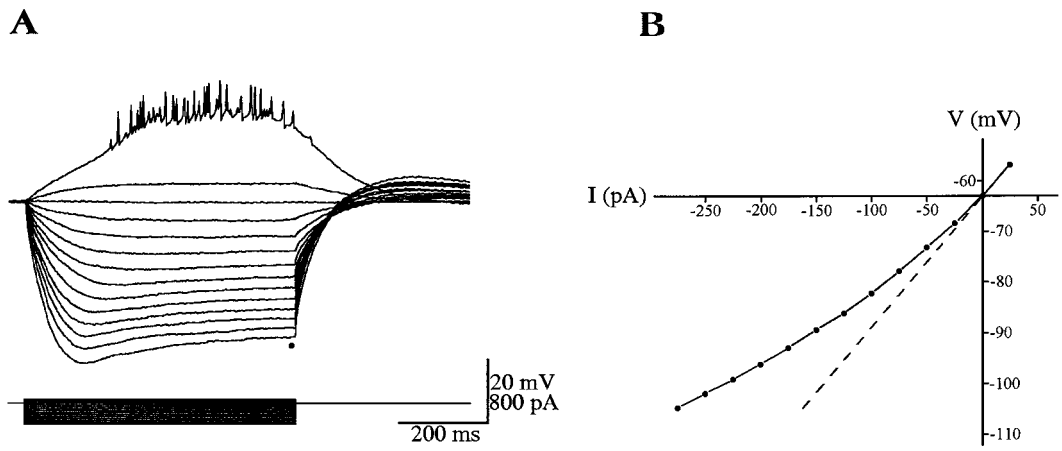

Fig. 2. Responses of a rat geniculate interneuron to current injections. (A) Step hyperpolarizing current injections revealed an inward rectification in a geniculate interneuron. Note that the recording traces were averaged five times. The *I–V* relationship at the point indicated by a dot in A is plotted in B. The dashed line is a linear line. The resting potential of this cell was −63 mV and the access resistance of the recording was 19 MΩ.

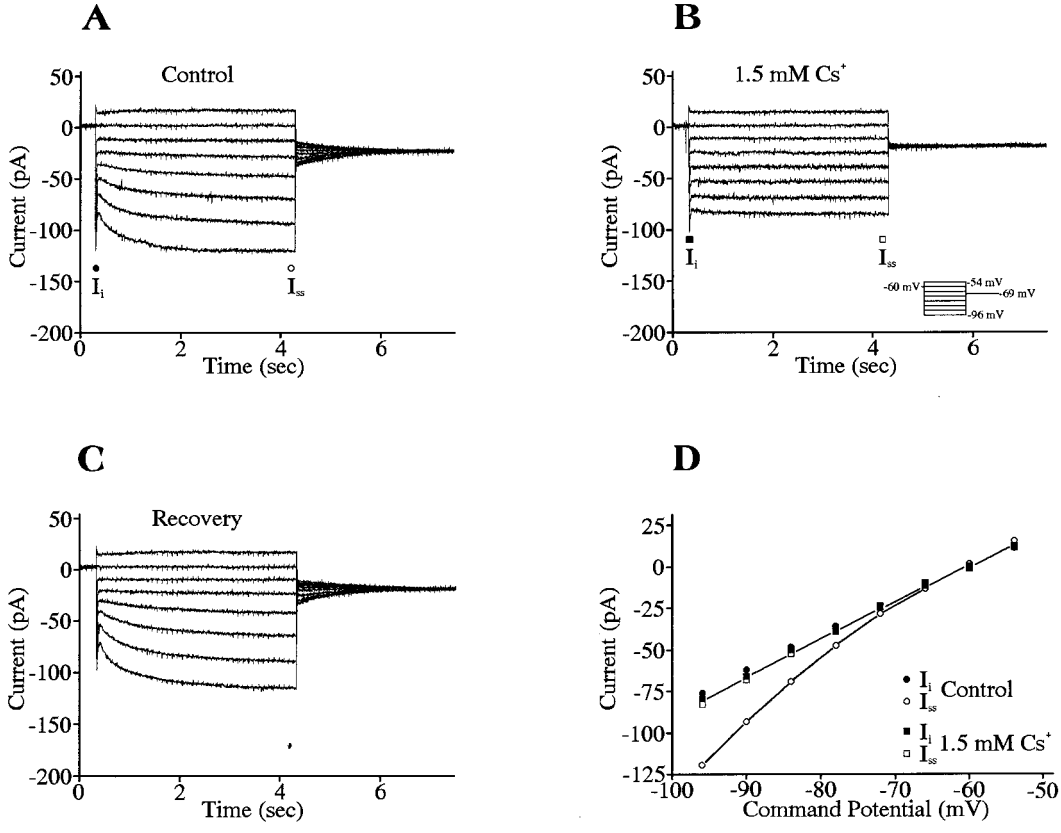

Fig. 3. Hyperpolarization-activated slow inward currents in a geniculate interneuron. (A) Hyperpolarizing voltage steps revealed slowly activated inward currents in the interneuron. (B) The inward currents were largely blocked by 1.5 mM Cs^+ in the bath solution. (C) The inward currents recovered after the washout of Cs^+ in the bath solution. Insert in B shows the voltage protocol used in experiments in A–C. The holding potential between the trials was −60 mV. (D) *I–V* relationships for instantaneous currents (I_i, filled symbols) and steady-state currents (I_{ss}, open symbols) obtained by experiments in A and B. The resting membrane potential of this cell was − 67 mV and the access resistance of the recording was 24 MΩ.

directly measuring the membrane potential at which the slow I_h tail current reversed from being inward to being outward (Fig. 5E, F). In this case, I_h was first activated by stepping the voltage to − 105 mV. After the I_h-mediated slow current reached its maximal value, the voltage was stepped back to a

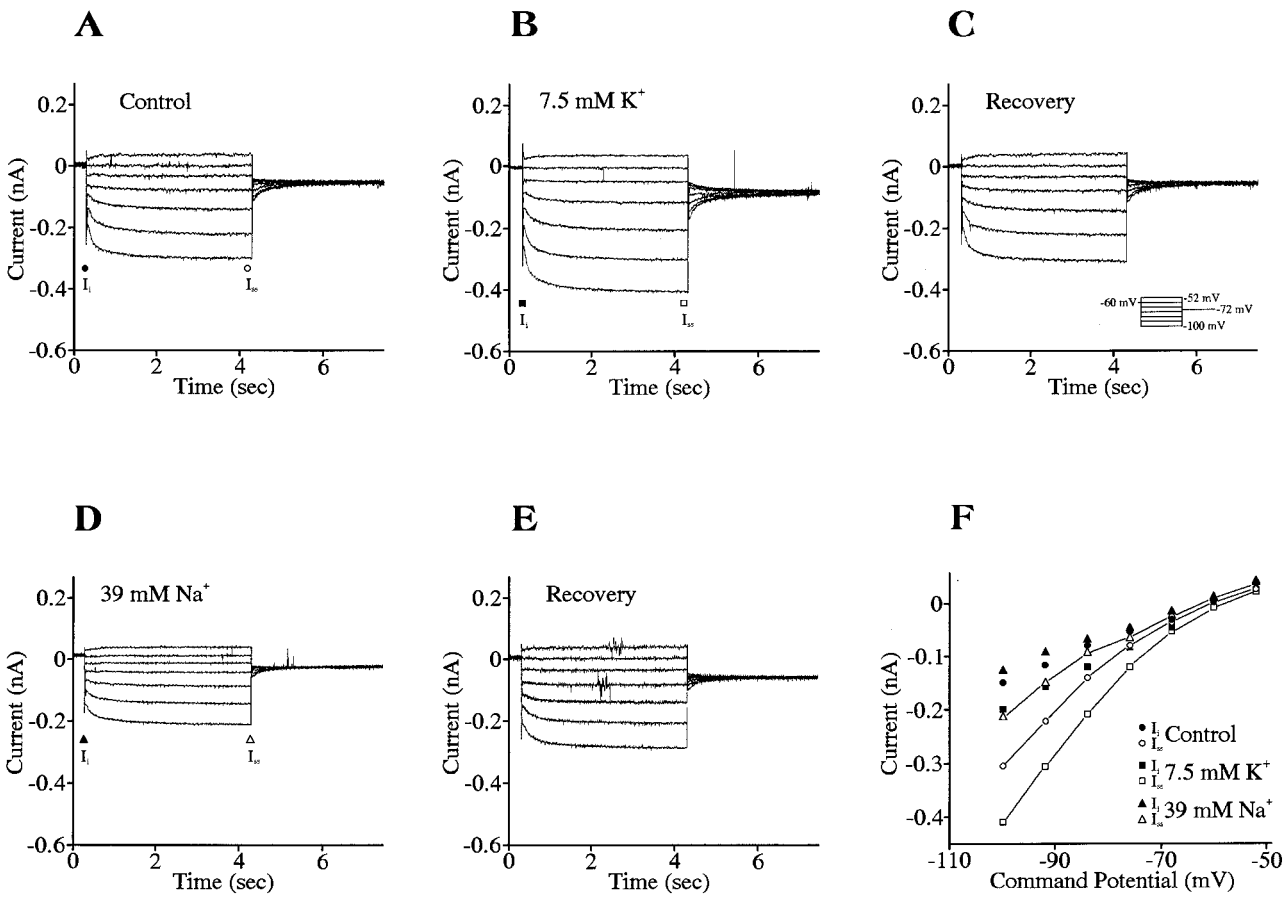

Fig. 4. Ionic selectivity of the slow inward currents in a geniculate interneuron. (A) Hyperpolarizing voltage steps revealed slowly activated inward currents. (B) Increasing K^+ concentration in the bath solution increased the amplitudes of slow inward currents. (C) The controls recovered after washing in the normal bath solution. (D) Current amplitude decreased when the concentration of Na^+ ions was decreased by substitution of $NMDG^+$ ions. (E) Recovery to control level after washing in the normal bath solution. Insert in C shows the voltage protocol used in experiments in A–E. The holding potential between the trials was −60 mV. (F) *I–V* relationships for instantaneous currents (I_i, filled symbols) and steady-state currents (I_{ss}, open symbols) obtained by experiments in A, B and D. The resting membrane potential of this cell was −63 mV and the access resistance of the recording was 15 MΩ.

series of test potentials from −85 to −45 mV (Fig. 5E). The amplitudes of the I_h tail currents were then plotted against test potentials to reveal the reversal potential (Fig. 5F). The mean reversal potential of I_h in five interneurons obtained using this method was −44.2 ± 3.0 mV.

Kinetics of I_h in interneurons

To better understand the action of I_h in interneurons, the kinetics of this current were also studied. Because I_h does not inactivate, the voltage dependence of steady-state activation can be directly measured from the amplitudes of I_h tail currents, where I_h was isolated from the instantaneous I_{leak}.[40] However, the full experiment was successful in only four interneurons whose I_h tail currents were large enough to be measured. The experiment showed that the amplitudes of I_h tail currents were dependent upon the preceding hyperpolarization (Fig. 5A, B). Plotting the amplitudes of I_h tail currents against the preceding command potentials resulted in the steady-state activation curve [$h_\infty(V)$] for I_h. The $h_\infty(V)$ was fitted by the Boltzmann equation (Fig. 6C), which provided estimates of the half-activation and steepness of $h_\infty(V)$ for I_h in interneurons to be −80.8 mV and −7.2, respectively.

Both activation and deactivation time constants of I_h were highly voltage dependent. These time constants were quantified by fitting the recording traces with exponential functions ($n = 5$). Single exponential processes satisfactorily described all activation and deactivation current traces, while two exponential functions sometimes improved the fit. To simplify the analysis and simulation, all current traces were fitted by single exponential functions. The time constants resulting from the fitting were plotted against the command potentials (Fig. 6D). These experimental data were then fitted with a bell-shaped function, which resulted in the

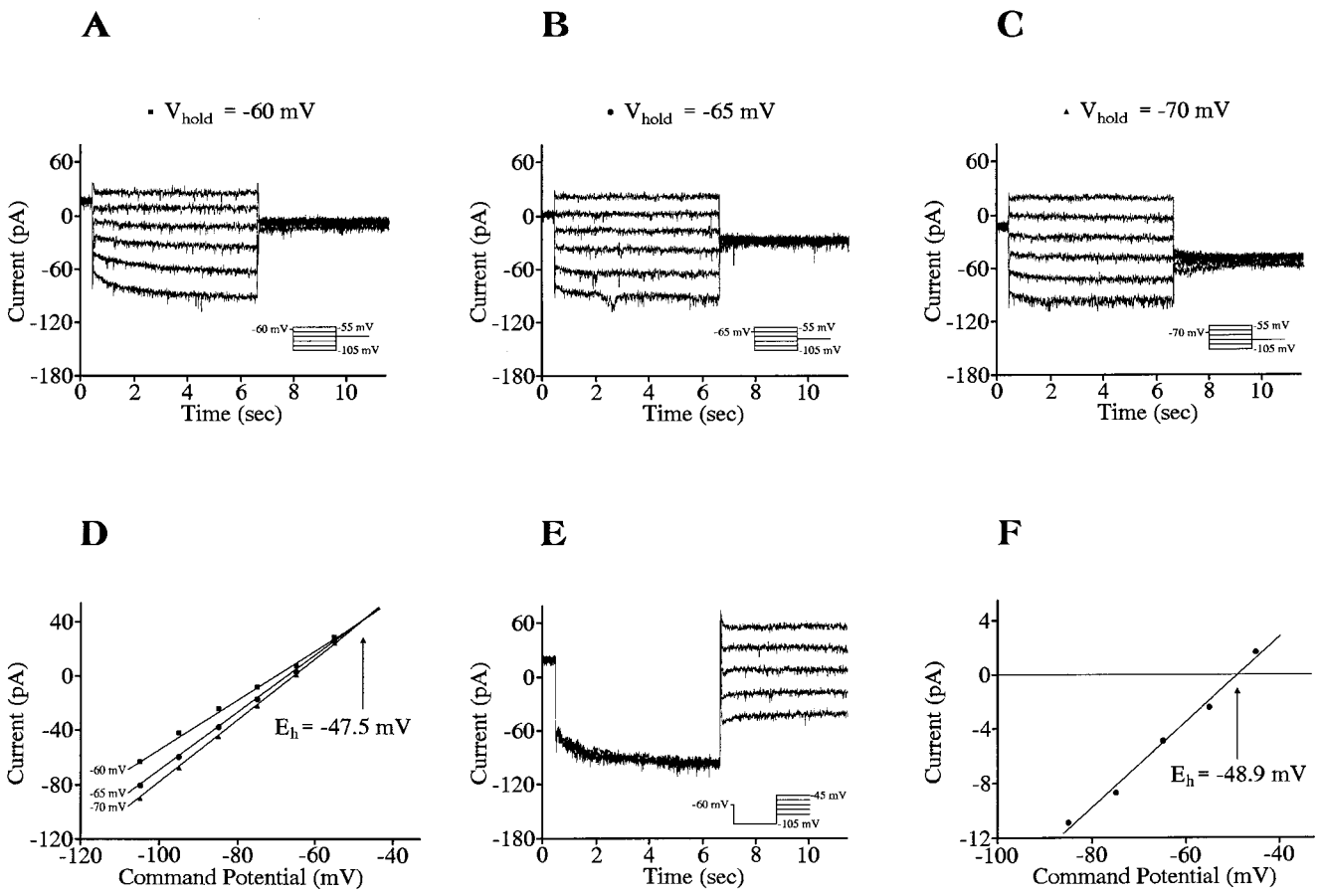

Fig. 5. Reversal potential of I_h in a geniculate interneuron. (A–C) The instantaneous responses evoked by a series of voltage steps in the same cell at different holding potentials. (D) Instantaneous *I–V* curves intersected at the reversal potential of I_h. (E) The slow inward current was initially activated by a hyperpolarizing voltage step and relaxed at different holding potentials. (F) Plotting the amplitudes of I_h tail currents against holding potentials revealed the reversal potential of I_h. Inserts in A–C and E show the voltage protocols. The holding potential between the trials was −60 mV. The resting membrane potential of this cell was −68 mV and the access resistance of the recording was 21 MΩ.

time constant function $\tau_h(V) = \exp[(V + 294)/30]/\{1 + \exp[(V + 74)/7.6]\}$.

To estimate the maximal conductance of I_h in interneurons, interneurons were initially held at −60 mV, where most of the I_h channels were deactivated, then stepped to −100 mV, where most of the I_h channels were slowly activated ($n = 28$; Fig. 7A; also see Fig. 6C). By measuring the difference between the instantaneous and steady-state inward currents, the maximal I_h-mediated inward currents were obtained. The amplitudes of I_h currents exhibited a scattered distribution between 12.8 and 159.5 pA, with a mean value of 56.6 ± 32.1 pA (Fig. 7B). This gave a maximal I_h conductance of 1.02 nS, assuming its reversal potential to be −44 mV {i.e. $g = I/(V_m - E_h) = -57$ pA/[−100 mV − (−44 mV)] = 1.02 nA}. This conductance value might be slightly underestimated because I_h was activated by the commanding hyperpolarizing voltage step from − 60 mV, where about 5% of I_h channels were already activated (see Fig. 6C). The inward currents were correlated with the instantaneous I_{leak} currents (Fig. 7C; $r = 0.649$, $P < 0.0005$, ANOVA), suggesting that if an interneuron has a large I_{leak} conductance, it will also have a large I_h conductance, and vice versa. Figure 7D shows the distribution of the ratio of I_h in total inward current. As expected, this distribution is more concentrated, ranging from 17.4% to 49.6% and having a mean value of 31.5 ± 8.7%.

Simulation of I_h in a model interneuron

A simulation was then performed on a model interneuron, using the I_h kinetics obtained in the voltage-clamp study, to test whether the I_h alone was sufficient to produce the inward rectification found in geniculate interneurons (Fig. 8). As with voltage-clamp recording on geniculate interneurons, the model neuron also responded to the hyperpolarization voltage steps with slowly activated inward currents (Fig. 8A). In addition, in current-clamp mode, the model cell formed voltage sags back

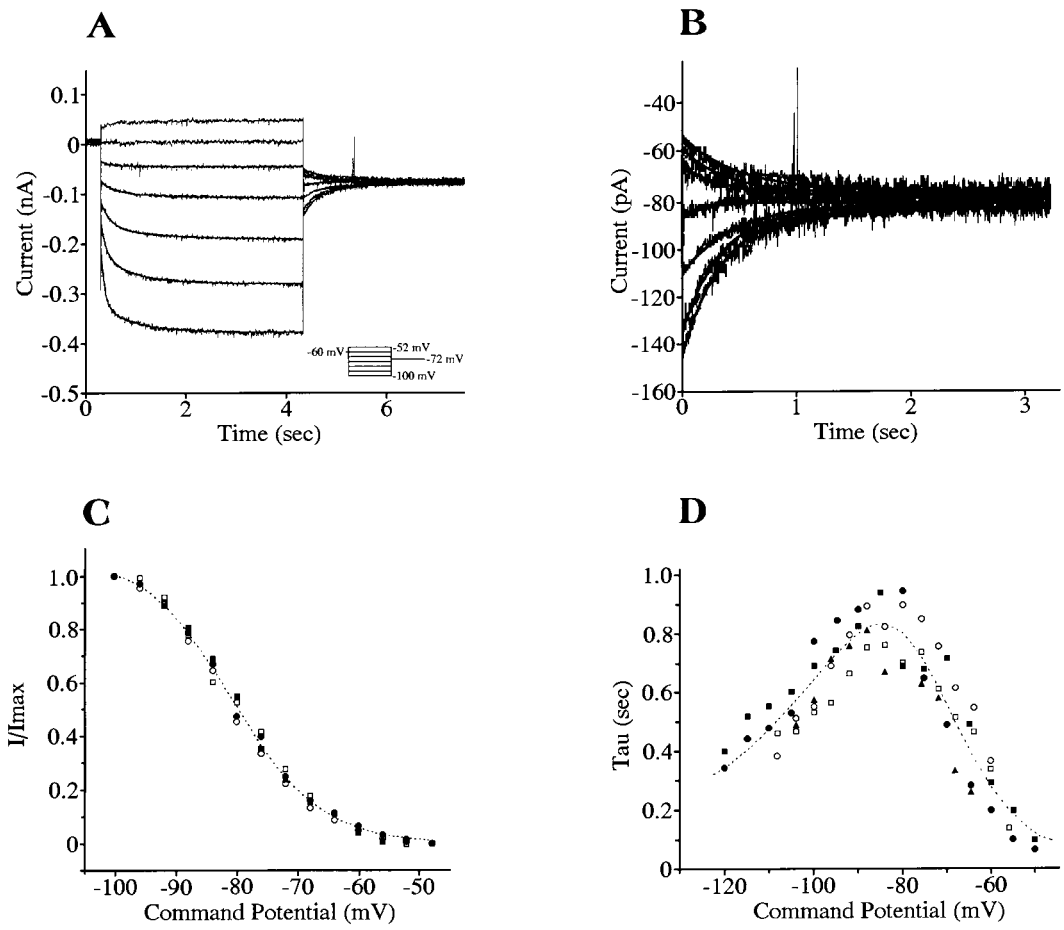

Fig. 6. Activation and deactivation kinetics of I_h in geniculate interneurons. (A) I_h was activated by hyperpolarizing voltage steps in a geniculate interneuron. I_h tail currents are expanded in B. Note that the two exponential and single exponential fitting curves are superimposed on the slow inward current traces (A) and tail current traces (B), respectively. The resting potential of this cell was −63 mV and the access resistance of the recording was 14 MΩ. (C) The amplitudes of the instantaneous I_h tail currents, obtained from four geniculate interneurons, were plotted against the preceding hyperpolarizing command voltage potentials. The dashed line is the best fit for the function $h_\infty(V)$. (D) Activation and deactivation time constants of I_h currents, obtained from five geniculate interneurons, were plotted against the command voltage potentials. The dashed line is the best fit for the function $\tau_h(V)$. The different symbols in C and D represent the data obtained from different neurons.

toward the resting potential during hyperpolarizations (Fig. 8B). Figure 8A and B are based on the average conductance seen experimentally and are not based on the specific data in any of the previous figures. Figure 8C shows the *I–V* curve for this model (filled circles), as well as results from models utilizing the maximum (open squares) and minimum (filled squares) conductances observed. This range encompasses the experimental data illustrated in the previous figures. The results further support the idea that I_h is the major reason for the anomalous *I–V* relationship in interneurons.

The steady-state activation curve of I_h indicates that about 20% of I_h channels are activated at the resting membrane potential in geniculate interneurons *in vitro* (see Fig. 6C), suggesting that I_h may be involved in determining the basic membrane properties and in modulating the postsynaptic responses. We thus modeled small signal-evoked responses in the presence and absence of I_h. Inserting I_h from the model shifted the resting membrane potential by 3.5 mV in the depolarizing direction. This was associated with a decrease in the input resistance by 29%. The membrane time constant decreased slightly due to the increased resting conductance. Interestingly, the results were the same for either small hyperpolarizations or small depolarizations. With hyperpolarization, I_h turned on, producing an inward current that resisted the hyperpolarization. With depolarization, I_h turned off, reducing the resting inward current and hence resisting the depolarization as well. In this way, I_h provides negative feedback that stabilizes the resting membrane potential against small deviations.

DISCUSSION

In the present whole-cell recording study, we

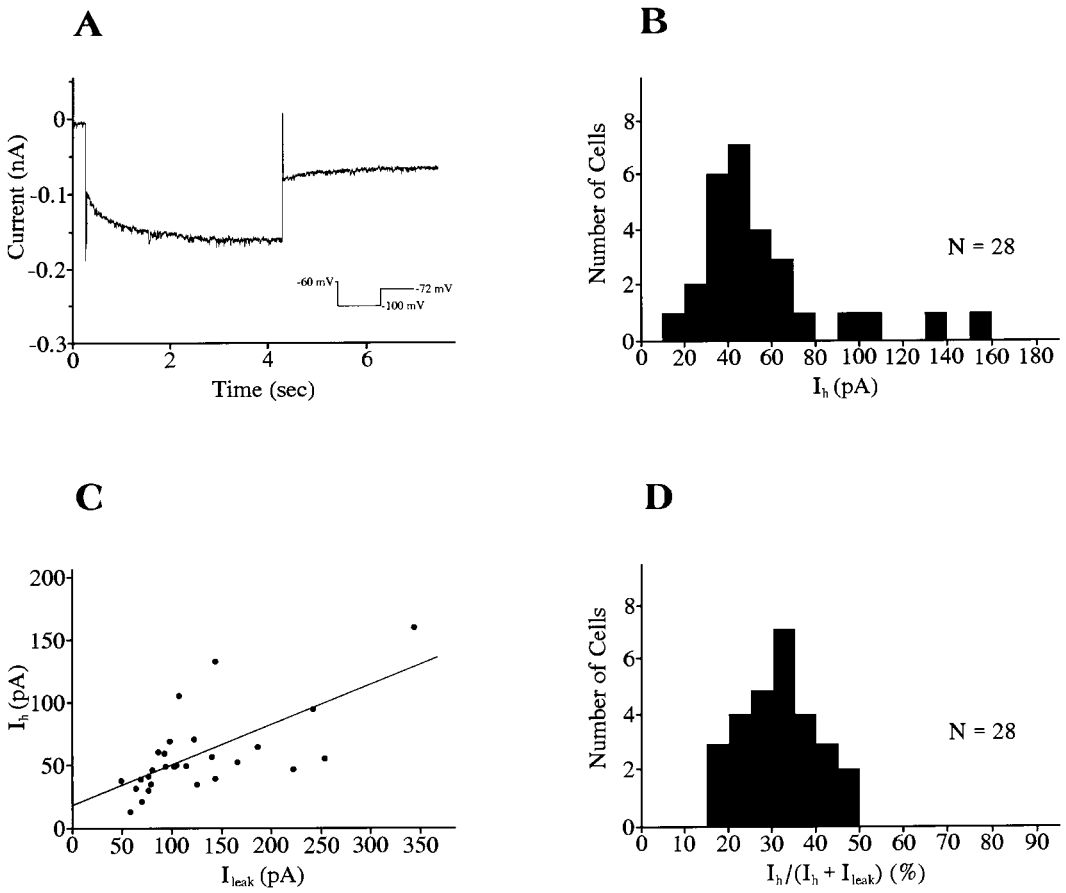

Fig. 7. Conductance of I_h in geniculate interneurons. (A) A hyperpolarizing voltage step from −60 to −100 mV activated I_h-mediated slow current in a geniculate interneuron. The holding potential before the trial was −60 mV. The resting membrane potential of this cell was −67 mV and the access resistance of the recording was 19 MΩ. (B) The histograms show a large variance in the amplitude of I_h-mediated current in geniculate interneurons. (C) The amplitude of I_h-mediated slow current was correlated with the amplitude of instantaneous I_{leak} current in interneurons. The line is the regression line. (D) Frequency distribution showing reduced variance when I_h amplitude is normalized by I_{leak} amplitude in the same cell. *N* is the total number of cells sampled in the histograms.

found that geniculate interneurons consistently exhibited a depolarizing "sag" in response to hyperpolarizing current pulses. We further demonstrated that the inward rectification underlying the sag was due to the hyperpolarization-activated conductance, I_h. In addition to I_h, deactivation of potassium conductances, such as I_M, may also contribute to inward rectification.[1] However, it seems unlikely that potassium conductances are substantially involved in the inward rectification in interneurons, since the slow inward currents were not reversed at − 100 mV, the potassium equilibrium potential. In addition, pharmacological experiments showed that the slow inward currents were insensitive to tetraethylammonium and 4-aminopyridine, but were largely blocked by low concentrations of Cs^+, arguing against the involvement of potassium conductances. Furthermore, computer simulation showed that I_h parameters obtained from voltage clamp were entirely consistent with the depolarizing sag seen in current clamp. Therefore, the contributions from potassium conductances to the inward rectification, if they do exist, must be very small.

Use of single-electrode voltage clamp in small cells

The small soma size of thalamic interneurons made recording from them difficult and necessitated the use of correspondingly small electrodes. Such small electrodes have a relatively high resistance to current flow, causing errors due to the voltage being measured through a voltage divider between the electrode's access resistance and the varying membrane resistance of the cell itself. To some extent, this can be compensated for by sourcing or sinking excess current, which effectively pushes the voltage beyond that measured through the electrode. There will be some remaining irreducible error which affects our estimates of the voltages at which I_h turns on and at which it saturates. By Ohm's law, this voltage error will be the product

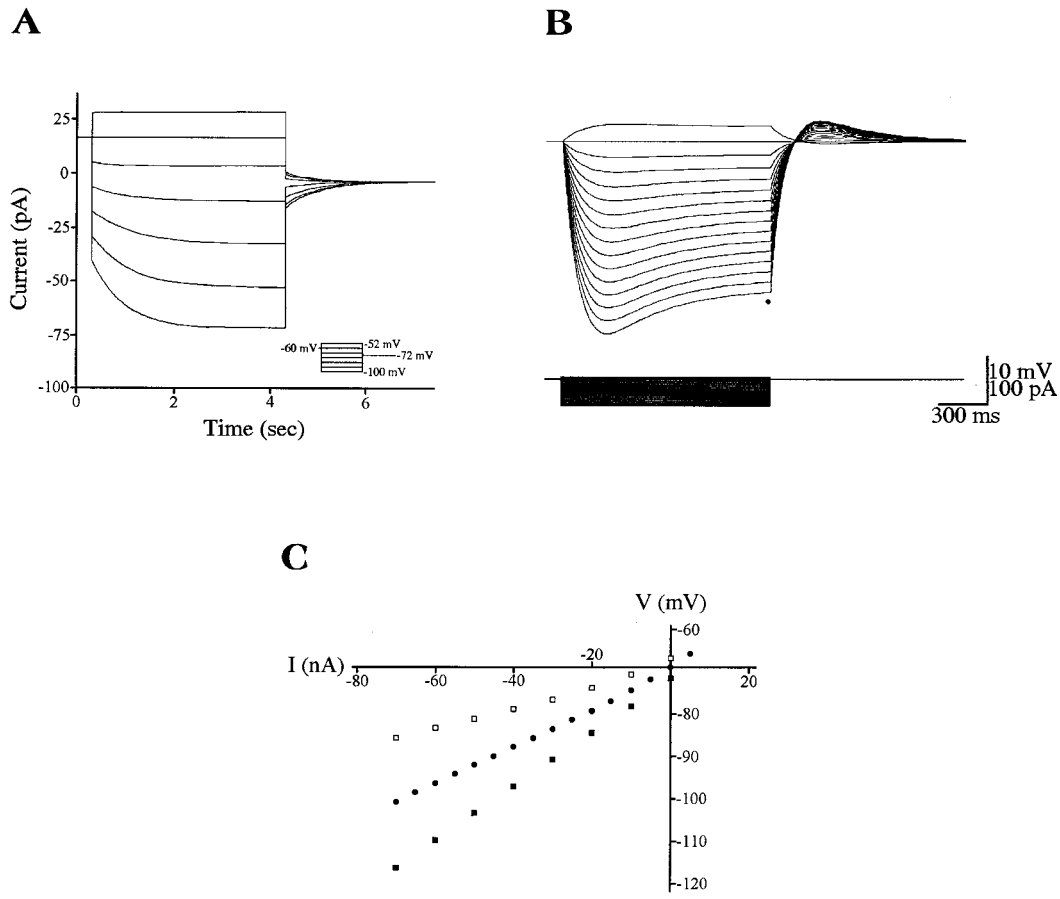

Fig. 8. Simulation of the *I–V* relationship in a model thalamic interneuron. (A) Voltage-clamp simulations of I_h-mediated slow inward currents in the model cell using the mean value of I_h conductance (0.13 mS/cm^2). The holding potential between the trials was −60 mV. (B) Current-clamp simulation of I_h-mediated inward rectification in the same model cell. (C) Summary *I–V* curves, derived from current-clamp simulations, for three models corresponding to the range of conductance values measured physiologically: mean I_h conductance shown in A and B (filled circles), maximum I_h conductance (open squares) and minimum I_h conductance (filled squares). The *I–V* values were obtained at the end of the current step (e.g., dot in B).

of the access resistence and the injected current. Therefore, the error will be worse for determination of I_h maximal opening, since these data points are determined using the highest currents. This will then tend to make the steady-state $I–I_{max}$ curve (Fig. 6C) appear slightly less steep. Additionally, the entire curve will be shifted slightly to the left. However, in most of our recordings, the errors were minimal. For the worst case of Fig. 6, the uncompensated error at the channel saturation is ~5.2 mV (370 nA, ×14 MΩ). With compensation we would estimate this error to be <1.6 mV. Uncompensated error at near channel threshold would be even smaller and would be brought down to a negligible value with compensation.

Comparison with other studies

An early study reported that geniculate interneurons had a relatively linear *I–V* relationship,[28] which led to the conclusion that I_h was absent in local interneurons in the thalamus.[48] However, the cells were studied with short current pulses, which would not have revealed the effects induced by slow conductances, such as I_h. Indeed, other studies, using longer pulses, showed that some geniculate interneurons generated an evident depolarizing sag back toward the resting membrane potential during hyperpolarization and had a non-linear *I–V* relationship.[32,42,58] Our findings that geniculate interneurons respond to hyperpolarizing current steps with an inward rectification are consistent with these studies, although we report this effect in all, rather than a minority, of our cells.

The reasons for this discrepancy in incidence may arise from differences in technique, as we used the whole-cell recording technique and previous studies used sharp electrodes, which may introduce a non-selective leak conductance.[51] Consistent with this idea, we find much higher values for input resistance than were reported in the sharp electrode studies. Under conditions of high input resistance, the relatively small I_h current in interneurons (see below) would result in fairly large deflections in voltage,

whereas the effect might be shunted (or simply too small to see) under conditions of lower input resistance.

The maximal conductance of I_h in interneurons appears to be smaller than that described in other cell types, where values of 2–10 nS have generally been reported. In thalamocortical cells, in particular, a maximal I_h conductance of 10–40 nS was found with a sharp electrode[33] or 3–15 nS with a patch electrode (our unpublished data; also see Ref. 9). TRN cells, on the other hand, appear to have no I_h channels.[5,10] Despite its small maximal conductance, I_h in interneurons can produce a pronounced depolarizing sag with hyperpolarizing current clamp. This is possibly due to the high input impedance of interneurons, which require less current to produce a noticeable effect. Our simulation was able to confirm the internal consistency of our data by demonstrating that the conductance value we calculated under voltage clamp could fully explain the effect observed under current clamp.

Functional considerations

A variety of complex functions have been suggested for I_h.[6,28,40] For example, in many cell types, including thalamocortical cells, I_h plays a key role in generating and pacing intrinsic oscillations.[23,33,49] While interneurons also have an intrinsic oscillation,[58,64] I_h appears not to be involved, since the oscillation occurs at depolarized levels, out of the activation range of I_h.

I_h is also implicated in more fundamental cellular functions,[33,40] and several observations suggest that I_h is indeed involved in basic membrane properties of interneurons. For example, I_h has a prominent maximal conductance with about 20% of channels activated at the resting membrane potential, and the maximal conductance of I_h is correlated with I_{leak}, suggesting that, as with I_{leak}, I_h also plays a crucial role in determining the basic membrane properties. Our modeling results indicate that I_h is implicated in damping deviations from the resting membrane potential. In addition, the input resistance decreased with hyperpolarization, since equivalent current injection resulted in reduced voltage change due to the increase in I_h. Similarly, the input resistance increased with depolarization due to a decrease in voltage change with decrease in I_h. At the same time, the time constant shortened, since a smaller voltage deflection was required to reach the appropriate percentage of the final value. These I_h-mediated alterations in membrane properties will determine how the interneurons integrate and respond to synaptic stimuli.[8,64] Furthermore, I_h can be activated by inhibitory postsynaptic potentials and afterhyperpolarizations, and in turn, I_h can curtail the amplitude and time-course of the inhibitory postsynaptic potentials and afterhyperpolarizations;[18,29,45,50,60] this conductance is likely involved in modulating the firing characteristics of interneurons.

An important property of I_h is that its kinetics can be modulated by a variety of neuromodulators,[40] thus providing a mechanism for modulating these fundamental membrane properties. In LGN thalamocortical cells, acetylchlorine, noradrenaline, serotonin, histamine and nitric oxide increase the maximal conductance of I_h and positively shift its activation curve,[34,35,39,66] while other substances (e.g., adenosine) do the opposite.[41] At present, it is not clear what effects the various neuromodulators may have on I_h in interneurons (cf. Ref. 42). However, if interneuron I_h channels can be modulated, this could have pronounced effects on the fundamental properties of the cells.

CONCLUSIONS

Our *in vitro* data suggest that the hyperpolarization-activated cation conductance, I_h, is likely to play an important role in modulating the electrophysiological behaviors of interneurons. Since interneurons are able to provide complicated forms of inhibition on thalamocortical cells,[2,11,14,22,44,48] it will be interesting to further study how I_h regulates the firing patterns in interneurons and the interneuron-mediated inhibition in thalamocortical cells.

Acknowledgements—We thank Drs Gerard Borst, Fu-Sun Lo, Lonnie Wollmuth and Ling-Gang Wu for their critical comments on this manuscript. This work was supported in part by fellowships from ONR/NIMH and the Neuroscience Training Program of the University of Wisconsin (J.J.Z.). Additional support came from NEI (D.J.U.) and NINDS (W.W.L.) grants and from the VA (W.W.L.).

REFERENCES

1. Adams P. R., Brown D. A. and Constanti A. (1982) M-currents and other potassium currents in bullfrog sympathetic neurones. *J. Physiol.* **330,** 537–572.
2. Ahlsén G., Lindström S. and Lo F.-S. (1984) Inhibition from the brain stem of inhibitory interneurones of the cat's dorsal lateral geniculate nucleus. *J. Physiol.* **347,** 593–609.
3. Ahlsén G., Lindström S. and Lo F.-S. (1985) Interaction between inhibitory pathways to principal cells in the lateral geniculate nucleus of the cat. *Expl Brain Res.* **58,** 134–143.
4. Avanzini G., de Curtis M. and Spreafico R. (1989) Intrinsic properties of nucleus reticularis thalami neurons of the rat studied *in vitro*. *J. Physiol.* **416,** 111–122.
5. Bal T. and McCormick D. A. (1993) Mechanisms of oscillatory activity in guinea-pig nucleus reticularis thalami *in vitro*. A mammalian pacemaker. *J. Physiol.* **468,** 669–691.

6. Banks M. I., Pearce R. A. and Smith P. H. (1993) Hyperpolarization-activated cation current (I_h) in neurons of the medial nucleus of the trapezoid body: voltage-clamp analysis and enhancement by norepinephrine and cAMP suggest a modulatory mechanism in the auditory brain stem. *J. Neurophysiol.* **70,** 1420–1432.
7. Blanton M. G., LoTurco J. J. and Kriegstein A. R. (1989) Whole cell recording from neurons in slices of reptilian and mammalian cerebral cortex. *J. Neurosci. Meth.* **30,** 203–210.
8. Bloomfield S. and Sherman S. M. (1989) Dendritic current flow in relay cells and interneurons of the cat's lateral geniculate nucleus. *Proc. natn. Acad. Sci. U.S.A.* **86,** 3911–3914.
9. Budde T., Biella G., Munsch T. and Pape H.-C. (1997) Lack of relation of intracellular Ca of the hyperpolarization-activated cation current in rat thalamic neurons. *J. Physiol.* **503,** 79–85.
10. Contreras D., Curró Dossi R. and Steriade M. (1993) Electrophysiological properties of cat reticular thalamic neurones *in vivo*. *J. Physiol.* **470,** 273–294.
11. Curró Dossi R., Paré D. and Steriade M. (1992) Various types of inhibitory postsynaptic potentials in anterior thalamic cells are differentially altered by stimulation of laterodorsal tegmental cholinergic nucleus. *Neuroscience* **47,** 279–289.
12. Destexhe A., Contreras D., Steriade M., Sejnowski T. J. and Huguenard J. R. (1996) *In vivo, in vitro*, and computational analysis of dendritic calcium currents in thalamic reticular neurons. *J. Neurosci.* **16,** 169–185.
13. Edward F. A., Konnerth A., Sakmann B. and Takahashi T. (1989) A thin slice preparation for patch clamp recordings from neurons of the mammalian central nervous system. *Pflügers Arch.* **414,** 600–612.
14. Eysel U. T., Pape H.-C. and Van Schayck R. (1986) Excitatory and differential disinhibitory actions of acetylcholine in the lateral geniculate nucleus of the cat. *J. Physiol.* **370,** 233–254.
15. Gabbott P. L. A., Somogyi J., Stewart M. G. and Hamori J. (1985) GABA-immunoreactive neurons in the rat dorsal lateral geniculate nucleus: light microscopical observations. *Brain Res.* **346,** 171–175.
16. Gabbott P. L. A., Somogyi J., Stewart M. G. and Hamori J. (1986) A quantitative investigation of the neuronal composition of the rat dorsal lateral geniculate nucleus using GABA-immunocytochemistry. *Neuroscience* **19,** 101–111.
17. Grossman A., Lieberman A. R. and Webster K. E. (1973) A Golgi study of the rat dorsal lateral nucleus. *J. comp. Neurol.* **166,** 245–256.
18. Halliwell J. V. and Adams P. R. (1982) Voltage-clamp analysis of muscarinic excitation in hippocampal neurons. *Brain Res.* **250,** 71–92.
19. Hamill O. P., Narty A., Neher E., Sakmann B. and Sigworth F. J. (1981) Improved patch-clamp technique for high-resolution current recording from cells and cell-free membrane patches. *Pflügers Arch.* **391,** 85–100.
20. Hines M. L. (1993) A program for simulation of nerve equations with branching geometries. *Int. J. Bio-Med. Comput.* **24,** 55–68.
21. Horikawa K. and Armstrong W. E. (1988) A versatile means of intracellular labeling: injection of biocytin and its detection with avidin conjugates. *J. Neurosci. Meth.* **25,** 1–11.
22. Hu B., Steriade M. and Deschênes M. (1989) The effects of brainstem peribrachial stimulation on neurons of the lateral geniculate nucleus. *Neuroscience* **31,** 13–24.
23. Huguenard J. R. and McCormick D. A. (1992) Simulation of the currents involved in rhythmic oscillations in thalamic relay neurons. *J. Neurophysiol.* **68,** 1373–1383.
24. Huguenard J. R. and Prince D. A. (1992) A novel T-type current underlies prolonged Ca^{2+}-dependent burst firing in GABAergic neurons of rat thalamic reticular nucleus. *J. Neurosci.* **12,** 3804–3817.
25. Huguenard J. R. and Prince D. A. (1994) Intrathalamic rhythmicity studied *in vitro*: nominal T-current modulation causes robust antioscillatory effects. *J. Neurosci.* **14,** 5485–5502.
26. Jahnsen H. and Llinás R. (1984) Electrophysiological properties of guinea-pig thalamic neurons: an *in vitro* study. *J. Physiol.* **349,** 205–226.
27. Jones E. G. (1985) *The Thalamus.* Plenum, New York.
28. Leresche N., Lightowler S., Soltesz I., Jassik-Gerschenfeld D. and Crunelli V. (1991) Low-frequency oscillatory activities intrinsic to rat and cat thalamocortical cells. *J. Physiol.* **441,** 155–174.
29. Maccaferri G. and McBain C. J. (1996) The hyperpolarization-activated current (I_h) and its contribution to pacemaker activity in rat CA1 hippocampal stratum oriens–alveus interneurones. *J. Physiol.* **497,** 119–130.
30. Major G., Larkman A. U., Jonas P., Sakmann B. and Jack J. J. (1994) Detailed passive cable models of whole-cell recorded CA3 pyramidal neurons in rat hippocampal slices. *J. Neurosci.* **14,** 4613–4638.
31. McCormick D. A. (1992) Neurotransmitter actions in the thalamus and cerebral cortex and their role in neuromodulation of thalamocortical activity. *Prog. Neurol.* **39,** 337–388.
32. McCormick D. A. and Pape H.-C. (1988) Acetylcholine inhibits identified interneurons in the cat lateral geniculate nucleus. *Nature* **334,** 246–248.
33. McCormick D. A. and Pape H. C. (1990) Properties of a hyperpolarization-activated cation current and its role in rhythmic oscillation in thalamic relay neurones. *J. Physiol.* **431,** 291–318.
34. McCormick D. A. and Pape H. C. (1990) Noradrenergic and serotonergic modulation of a hyperpolarization-activated cation current in thalamic relay neurones. *J. Physiol.* **431,** 319–342.
35. McCormick D. A. and Williamson A. (1991) Modulation of neuronal firing mode in cat and guinea pig LGNd by histamine: possible cellular mechanisms of histaminergic control of arousal. *J. Neurosci.* **11,** 3188–3199.
36. Norton T. T. and Gudwin D. W. (1992) Inhibitory GABAergic control of visual signals at the lateral geniculate nucleus. *Prog. Brain Res.* **90,** 192–217.
37. Ohara P. T., Lieberman A. R., Hunt S. P. and Wu J.-Y. (1983) Neural elements containing glutamic acid decarboxylase (GAD) in the dorsal lateral geniculate nucleus of the rat: immunohistochemical studies by light and electron microscopy. *Neuroscience* **8,** 189–244.
38. Ottersen O. P. and Storm-Mathisen J. (1984) Glutamine- and GABA-containing neurons in the mouse and rat brain, as demonstrated with a new immunocytochemical technique. *J. comp. Neurol.* **229,** 374–392.
39. Pape H.-C. (1992) Adenosine promotes burst activity in guinea-pig geniculocortical neurones through two different ionic mechanisms. *J. Physiol.* **447,** 729–753.
40. Pape H.-C. (1996) Queer current and pacemaker: the hyperpolarization-activated cation current in neurons. *A. Rev. Physiol.* **58,** 299–327.
41. Pape H.-C. and Mager R. (1992) Nitric oxide controls oscillatory activity in thalamocortical neurons. *Neuron* **9,** 441–448.
42. Pape H.-C. and McCormick D. A. (1995) Electrophysiological and pharmacological properties of interneurons in the cat dorsal lateral geniculate nucleus. *Neuroscience* **68,** 1105–1125.

43. Pape H.-C., Budde T., Mager R. and Kisvarday Z. F. (1994) Prevention of Ca^{2+}-mediated action potentials in GABAergic local circuit neurones of rat thalamus by a transient K^+ current. *J. Physiol.* **478,** 403–422.
44. Paré D., Curró Dossi R. and Steriade M. (1991) Three types of inhibitory postsynaptic potentials generated by interneurons in the anterior thalamic complex of cat. *J. Neurophysiol.* **66,** 1190–1204.
45. Schwindt P. C., Spain W. J. and Crill W. E. (1988) Influence of anomalous rectifier activation on hyperpolariaztions of neurons from cat sensorimotor cortex *in vitro*. *J. Neurophysiol.* **59,** 468–481.
46. Sherman S. M. and Koch C. (1986) The control of retinogeniculate transmission in the mammalian lateral geniculate nucleus. *Expl Brain Res.* **63,** 1–20.
47. Sherman S. M. and Guillery R. W. (1996) Functional organization of thalamocortical relays. *J. Neurophysiol.* **76,** 1367–1395.
48. Soltesz I. and Crunelli V. (1992) $GABA_A$ and pre- and post-synaptic $GABA_B$ receptor-mediated responses in the lateral geniculate nucleus. *Prog. Brain Res.* **90,** 151–169.
49. Soltesz I., Lightowler S., Leresche N., Jassik-Gerschenfeld D., Pollard C. E. and Crunelli V. (1991) Two inward currents and the transformation of low-frequency oscillations of rat and cat thalamocortical cells. *J. Physiol.* **441,** 175–197.
50. Spain W. J., Schwindt P. C. and Crill W. E. (1987) Anomalous rectification in neurons from cat sensorimotor cortex *in vitro*. *J. Neurophysiol.* **57,** 1555–1576.
51. Staley K. J., Otis T. S. and Mody I. (1992) Membrane properties of dentate gyrus granule cells: comparison of sharp microelectrode and whole-cell recordings. *J. Neurophysiol.* **67,** 1346–1358.
52. Steriade M., McCormick D. A. and Sejnowski T. J. (1993) Thalamocortical oscillations in the sleeping and aroused brain. *Science* **262,** 679–685.
53. Takashima S. (1976) Membrane capacity of squid giant axon during hyper- and depolarization. *J. Membrane Biol.* **27,** 21–39.
54. Uhlrich D. J., Tamamaki N., Murphy P. C. and Sherman S. M. (1995) Effects of brain stem parabrachial activation on receptive field properties of cells in the cat's lateral geniculate nucleus. *J. Neurophysiol.* **73,** 2428–2447.
55. von Krosigk M., Bal T. and McCormick D. A. (1993) Cellular mechanisms of a synchronized oscillation in the thalamus. *Science* **261,** 361–364.
56. Warren R. A., Agmon A. and Jones E. G. (1994) Oscillatory synaptic interactions between ventroposterior and reticular neurons in mouse thalamus *in vitro*. *J. Neurophysiol.* **72,** 1993–2003.
57. Webster M. J. and Rowe M. H. (1984) Morphology of identified relay cells and interneurons in the dorsal lateral nucleus of the rat. *Expl Brain Res.* **56,** 468–474.
58. Williams S. R., Turner J. P., Anderson C. M. and Crunelli V. (1996) Electrophysiological and morphological properties of interneurones in the rat dorsal lateral geniculate nucleus *in vitro*. *J. Physiol.* **490,** 129–147.
59. Wollmuth L. P. and Hille B. (1992) Ionic selectivity of I_h channels of rod photoreceptors in tiger salamanders. *J. gen. Physiol.* **100,** 749–765.
60. Zhu J. J. and Lo F.-S. (1996) Time course of inhibition induced by a putative saccadic suppression circuit in the dorsal lateral geniculate nucleus of the rabbit. *Brain Res. Bull.* **41,** 281–291.
61. Zhu J. J. and Lo F.-S. (1998) Control of recurrent inhibition of the lateral posterior–pulvinar complex by afferents from the deep layers of the superior colliculus of the rabbit. *J. Neurophysiol.* **80,** 1122–1131.
62. Zhu J. J. and Lo F.-S. (1997) Recurrent inhibitory interneurons of the rabbit's lateral posterior–pulvinar complex. *J. Neurophysiol.* **78,** 3117–3124.
63. Zhu J. J. and Uhlrich D. J. (1997) Nicotinic receptor-mediated responses in relay cells and interneurons in the rat lateral geniculate nucleus. *Neuroscience* **80,** 191–202.
64. Zhu J. J., Lytton W. W., Xue J.-T. and Uhlrich D. J. (1999) An intrinsic oscillation in interneurons of the rat lateral geniculate nucleus. *J. Neurophysiol.* **81,** 702–711.
65. Zhu J. J., Uhlrich D. J. and Lytton W. W. (1999) Burst firing in identified interneurons of the rat lateral geniculate nucleus. *Neuroscience* **91,** 1445–1461.
66. Zhu J. J. and Uhlrich D. J. (1998) Cellular mechanisms underlying two muscarinic receptor-mediated depolarizing responses in relay cells of the rat lateral geniculate nucleus. *Neuroscience* **87,** 767–781.

(*Accepted* 16 *December* 1998)